Nanostructured Lanthanide-Doped Lu_2O_3 Obtained by Propellant Synthesis

Stefano Polizzi,*,† Stefania Bucella,† Adolfo Speghini,‡ Fiorenzo Vetrone,§ Rafik Naccache,§ John C. Boyer,§ and John A. Capobianco§

Dipartimento di Chimica Fisica, Università di Venezia, Via Torino 155/b, 30172 Venezia-Mestre, Italy, Dipartimento Scientifico e Tecnologico, Università di Verona, Ca' Vignal, Strada le Grazie 15, 37134 Verona, Italy, and Department of Chemistry and Biochemistry, Concordia University, 1455 de Maisonneuve Blvd. W, Montreal, QC; H3G-1M8, Canada

Received November 5, 2003. Revised Manuscript Received January 22, 2004

$Lu_{1.98}Ln_{0.02}O_3$ (Ln = Nd, Eu, and Er) powders obtained by propellant synthesis were characterized using XRD, SAXS, TEM, and SEM. Samples have a very porous, open morphology with fractal scaling properties. The building blocks of the fractal aggregates are 60−90 nm lanthanide-doped cubic Lu_2O_3 crystalline particles, which exhibit changes in the lattice parameter proportional to the lanthanide ionic radius. The NIR luminescence spectrum of nanocrystalline Lu_2O_3:Nd^{3+} was measured and emission was observed from the $^4F_{3/2}$ excited state to the ^4I_J (9/2, 11/2, 13/2, 15/2) state. The spectral features are very similar to those of a bulk material of identical composition prepared for comparison, though with a noticeable difference in the relative intensity of the $^4F_{3/2} \rightarrow {}^4I_{9/2}$ and $^4F_{3/2} \rightarrow {}^4I_{11/2}$ transitions. The spectroscopic-quality parameter (X) for nanocrystalline samples was calculated and was found to be higher than for the bulk.

Introduction

Lutetium oxide (Lu_2O_3) is an excellent candidate for lanthanide ion substitution due to its favorable physical properties, such as high melting point, phase stability, and low thermal expansion.[1] However, due to the physical nature of this sesquioxide, the growth of a high optical quality Lu_2O_3:Ln^{3+} single crystal is an arduous process, and thus solid-state methods are employed to synthesize polycrystalline Lu_2O_3:Ln^{3+} with particle sizes in the tens of micrometers range. In the past few years, methods have been developed that are able to create with relative ease the same materials in the nanometer range.[2−6] One of such method involves a combustion process between metal nitrates and an organic fuel, which is called propellant synthesis, because the starting system is an aqueous solution. This is a relatively fast and economical way to prepare Lu_2O_3:Ln^{3+} phosphors with nanometric particle sizes.

It has been shown that the nanocrystalline materials may have properties that differ from those of the same material in the bulk phase. In the case of nanocrystalline sesquioxides doped with trivalent lanthanide ions, largely different optical properties have been previously demonstrated, including differences in luminescence efficiency, excited-state dynamics, and up conversion.[7−9] These enhanced properties have important implications in the technological domain where many of today's standard devices are smaller than their predecessors. Consequently, there exists a need for new, far more efficient emissive materials with smaller sizes, to meet the demand of current technology.

In the present paper, Lu_2O_3:Ln^{3+} (Ln = Nd, Eu, and Er) nanocrystals synthesized by the propellant process are studied. A detailed physical characterization is presented, as well as some basic luminescence studies.

Experimental Details

Samples. Lu_2O_3 nanocrystals doped with 1 mol % Ln_2O_3 ($Lu_{1.98}Ln_{0.02}O_3$, where Ln = Nd, Eu and Er) were prepared using a propellant synthesis.[2,3] The process involves the exothermic reaction between a metal nitrate (oxidizer) and an

* Corresponding author. Tel: +39041 2346722. Fax: +39041 2346747. E-mail: polizzi@unive.it.
† Università di Venezia.
‡ Università di Verona.
§ Concordia. University

(1) Lu, J.; Takaichi, K.; Uematsu, T.; Shirakawa, A.; Musha, M.; Ueda, K.; Yagi, H.; Yanagitani, T.; Kaminskii, A. A. *Appl. Phys. Lett.* **2002**, *81*(23), 4324.
(2) Tao, Y.; Zhao, G.; Zhang, W.; Xia, S. *Mater. Res. Bull.* **1997**, *32*(5), 501.
(3) Tessari, G.; Bettinelli, M.; Speghini, A.; Ajò, D.; Pozza, G.; Depero, L. E.; Allieri, B.; Sangaletti, L. *Appl. Surf. Sci.* **1999**, *144−145*, 686.
(4) Sharma, P. K.; Jilavi, M. H.; Nass, R.; Schmidt, H. *J. Lumin.* **1999**, *82*(3), 187.
(5) Eilers, H.; Tissue, B. M. *Mater. Lett.* **1995**, *24*(4), 261.
(6) Konrad, A.; Fries, T.; Gahn, A.; Kummer, F.; Herr, U.; Tidecks, R.; Samwer, K. *Chem. Vap. Depos.* **1999**, *5*(5), 207.
(7) Capobianco, J. A.; Vetrone, F.; Boyer, J. C.; Speghini, A.; Bettinelli, M. *Opt. Mater.* **2002**, *19*(2), 259.
(8) Vetrone, F.; Capobianco, J. A.; Boyer, J. C.; Speghini, A.; Bettinelli, M. *J. Phys. Chem. B* **2003**, *106*(22), 5622.
(9) Williams, D. K.; Yuan, H.; Tissue, B. M. *J. Lumin.* **1999**, *83&84*, 297.

10.1021/cm0351240 CCC: $27.50
Published on Web 02/28/2004

organic fuel, such as glycine. The stoichiometric synthesis reaction is:

$$6M(NO_3)_3 + 10NH_2CH_2COOH + 18O_2 \rightarrow 3M_2O_3 + 5N_2 + 18NO_2 + 20CO_2 + 25H_2O$$

where M are Lu and Ln. The size of the nanopowders is greatly influenced by the reaction temperature, which can be controlled by adjusting the glycine-to-metal nitrate molar ratio.[2] The aqueous precursor solution was prepared by employing a glycine-to-metal nitrate molar ratio of 1.2:1. After the synthesis, the resulting material was fired at 500 °C for 1 h in order to decompose any residual nitrate ions. For comparison, a bulk sample with identical Nd^{3+} concentration ($Lu_{1.98}Nd_{0.02}O_3$) was prepared by intimately mixing the oxides Lu_2O_3 (Aldrich, 99.99%) and Nd_2O_3 (Aldrich, 99.99+ %), pressing the powders into pellets under 10 tons of pressure, and firing them in air at 1500 °C for 48 h. At this temperature, the optimum homogeneity was obtained. All lutetia samples were kept in air without any further precaution. The surface area obtained by BET measurements is 111 m^2/g.

Spectroscopy. The diffuse reflectance spectra in the medium-infrared (MIR) region were measured at room temperature using a Nicolet Magna 760 FTIR spectrometer with an aluminated mirror as a reference.

The near-infrared (NIR) emission spectra and decay times were acquired using the 488-nm line of the argon ion laser and recorded with a Jarrell-Ash $^3/_4$ m Czerny-Turner single monochromator in second order. A Stanford Research Systems SR540 optical chopper was used to modulate the 488-nm excitation wavelength. The signal was detected by a Northcoast EO-817P liquid nitrogen-cooled germanium detector connected to a computer-controlled Stanford Research Systems model SR510 lock-in amplifier. All spectroscopic measurements were carried out at room temperature.

SEM and TEM. Scanning electron microscopy (SEM) images were taken with a JEOL JSM 5600 LV electron microscopy. Samples were coated with a Pd/Au thin film, to avoid charging effects.

Transmission electron microscopy (TEM) images were taken with a JEOL 3010, operating at 300 kV, equipped with a Gatan slow-scan CCD camera (Mod. 794). The powder was dispersed in an isopropyl alcohol solution by a short sonication, and a 5 μm drop was deposited on a carbon holey film.

XRD. A Philips X'Pert vertical goniometer with Bragg−Brentano geometry, connected to a highly stabilized generator, was used for X-ray diffraction (XRD) analysis. Cu Kα (Ni-filtered) radiation, a graphite monochromator on the diffracted beam, and a proportional counter with pulse height discriminator were used. For the determination of the lattice parameters and Rietveld analysis, measurements in the 14°−140° range in 2θ (Bragg angle) were collected with a step size of 0.05° and 10 s per point for five runs of 10 s per each point and then averaged. The cubic unit-cell-edge values were calculated by using the angular peak position of 23 reflections in the 2θ range of 25°−85°. In accordance with Wagner,[10,11] the cell-edge value was extrapolated by applying a weighted least-squares linear fit to the cell-edge values calculated from the position of each single reflection as a function of $\cos\theta \cot\theta$. The peak position were obtained using a previously reported best-fitting procedure,[12,13] where each peak is described by a couple of constrained pseudo-Voigt functions ($K_{\alpha 1}$ and $K_{\alpha 2}$ profiles) and the background by a polynomial function.

The line-broadening analysis was carried out by the Warren-Averbach method[14,15] using the two 222/444 and 400/800 pairs of reflections. In accordance with this method, the following equation can be written for the Fourier transform $A(D)$ (D is the variable in direct space) of the fitted peak profile

$$\ln\left[A\left(D,\frac{1}{d_{hkl}^{\,2}}\right)\right] = \ln[A^s(D)] - \frac{2\pi\langle\epsilon^2(D)\rangle}{d_{hkl}^{\,2}}D^2 \qquad (1)$$

where hkl are the Miller indices, d_{hkl} is the interplanar spacing, $A^s(D)$ is the Fourier transform of the peak profile corrected for broadening caused by lattice disorder effects and $\langle\epsilon^2(D)\rangle$ is the mean square microstrain distribution. Thus, by using the Fourier coefficients of two different peaks belonging to the same family of crystallographic planes, the real distribution of crystallite dimensions, $A^s(D)$, and the corresponding distribution of microstrains can be obtained. Both distributions refer to the direction perpendicular to the (hkl) family of crystallographic planes. $A^s(D)$ is suitably averaged, to obtain the volume-weighted average crystallite size, $\langle D\rangle_v$. The value of $\langle\epsilon^2(D)\rangle$ at $\langle D\rangle_v/2$ is taken as a measure of the average microstrain. The instrumental broadening was previously deconvolved by using the Stokes' method, adapted to analytically defined profiles.

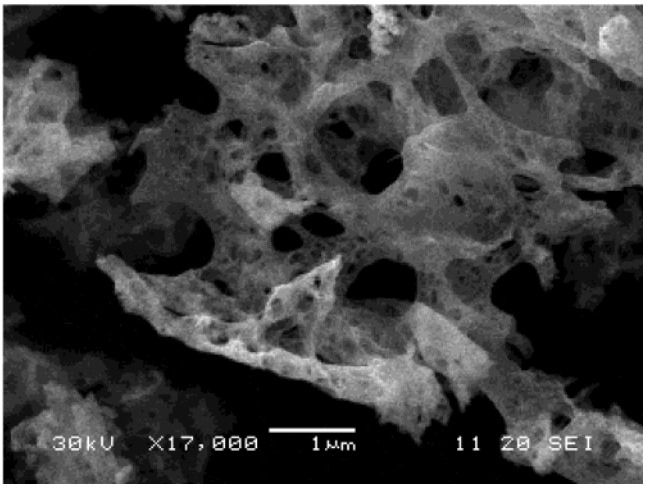

Figure 1. SEM image of a Lu_2O_3 sample, obtained by propellant synthesis.

SAXS. The small-angle X-ray scattering (SAXS) measurements were made using a Kratky (PAAR) camera, with an entrance slit of 25 μm. Nickel-filtered Cu Kα radiation, a pulse-height discriminator, and a proportional counter were used in the preset counting mode (2000 counts per angular step, repeated for at least 10 runs and finally averaged). The experimental intensities, $J(h)$, were corrected for absorption and air scattering ($h=4\pi \sin\vartheta/\lambda$, where λ is the radiation wavelength).

Results and Discussion

Morphology and Structure. In Figure 1, a typical SEM image is shown. All samples have a microscopic, open, spongelike morphology, similar to the one observed for the previously studied yttria powders,[16,17] which were prepared with a similar procedure. The same morphology is observed over different scales (see also the TEM images below), suggesting a fractal behavior.

XRD patterns (see Figure 2) indicate that, in all samples, the crystalline domains preserve the crystal-

(10) Wagner, C. N. J. In *Local Atomic Arrangements Studied by X-ray Diffraction*; Cohen, J. B., Hilliard, J. E., Eds.; Met. Soc. Conf. 36, Gordon & Breach: New York, 1966; p 9.
(11) Adler, R. P. I.; Wagner, C. N. J. *J. Appl. Phys.* **1962**, *33*, 3451.
(12) Enzo, S.; Polizzi, S.; Benedetti, A. *Z. Kristallogr.* **1985**, *170*, 275.
(13) Benedetti, A.; Fagherazzi, G.; Enzo, S.; Battagliarin, M. *J. Appl. Crystallogr.* **1988**, *21*, 543.
(14) Warren, B. E.; Averbach, B. L. *J. Appl. Phys.* **1950**, *21*, 595.
(15) Warren, B. E.; Averbach, B. L. *J. Appl. Phys.* **1952**, *23*, 497.
(16) Fagherazzi, G.; Polizzi, S.; Bettinelli, M.; Speghini, A. *J. Mater. Res.* **2000**, *15*(3), 586.
(17) Polizzi, S.; Fagherazzi, G.; Battagliarin, M.; Bettinelli, M.; Speghini, A. *J. Mater. Res.* **2001**, *16*, 146.

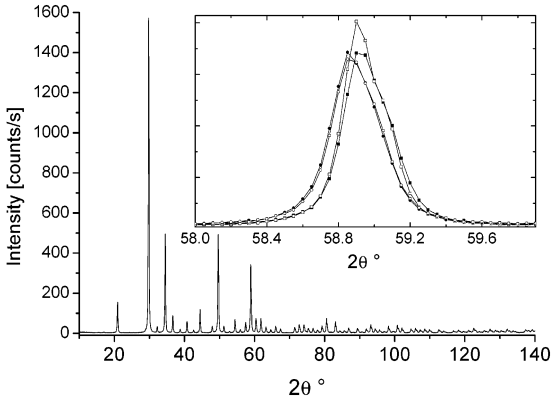

Figure 2. WAXS patterns of the Lu_2O_3 sample obtained by propellant synthesis and (inset) of the (622) peaks for doped and undoped samples (■, Lu_2O_3; □, $Lu_{1.98}Er_{0.02}O_2$; ○, $Lu_{1.98}Eu_{0.02}O_2$; ●, $Lu_{1.98}Nd_{0.02}O_2$) showing the peak shifts.

Table 1. Cubic Unit-Cell-Edge Values, *a*, and Crystallite Dimensions, $\langle D\rangle_v$, for Two Different Pairs of Reflections and Particles Dimension $2\pi/h_f$

		$\langle D\rangle_v$ (nm)		
sample	*a* (nm)	222/444	400/800	$2\pi/h_f$ (nm)
Lu_2O_3	1.03901(4)	34	34	65
$Lu_{1.98}Er_{0.02}O_3$	1.03921(4)	37	38	80
$Lu_{1.98}Eu_{0.02}O_3$	1.03969(4)	31	31	60
$Lu_{1.98}Nd_{0.02}O_3$	1.03970(5)	31	31	60

lographic structure of lutetia (Lu_2O_3, cubic system; space group *Ia*3) and that no other segregated phases are present, within the sensitivity of X-ray diffraction. Peak shifts are observed for the doped samples (see inset of Figure 2). The unit-cell-edge value, *a*, obtained for the undoped lutetia sample is exactly the one reported in the literature,[18] whereas a roughly linearly increase with the lanthanide ionic radius[19] is observed with doping (see Table 1). No significant amorphous fraction is present in the material.

A quantitative line-broadening analysis of the diffraction peaks indicates a crystallite average dimension in the 30−40 nm range along both the crystallographic directions analyzed (see Table 1), while no significant microstrains have been revealed.

On the other hand, SAXS data indicate that particles are actually larger, in the 60−80 nm range (see Table 1). This fact is discussed below in connection with TEM images.

As for the previously studied yttria samples,[16,17] SAXS data show two regions with constant slope with a crossover (see Figure 3). This trend is characteristic of a fractal behavior, the crossover indicating the size of the building blocks that make up the whole fractal structure. The slope of the low-angle part of the data is lower than 2 (corresponding to a slope of 3 for desmeared data), suggesting the mass-fractal behavior expected for multiparticle aggregates obtained in nonisothermal combustion-synthesis reactors.[20] This is consistent with values reported[21] for the formation of very

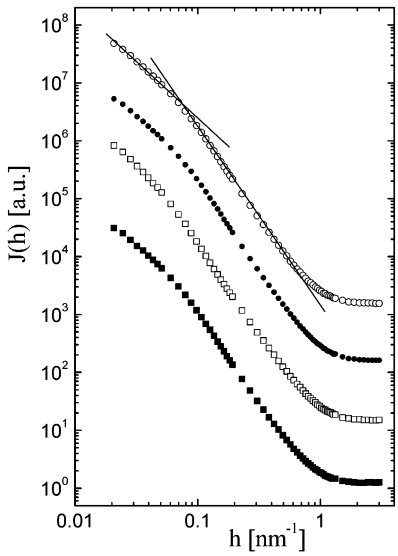

Figure 3. SAXS data in a log $J(h)$−log h plot: ■, Lu_2O_3; □, $Lu_{1.98}Er_{0.02}O_2$; ○, $Lu_{1.98}Eu_{0.02}O_2$; ●, $Lu_{1.98}Nd_{0.02}O_2$. Curves have been vertically shifted for greater clarity. The indicated slopes are only intended as a guide for the eye.

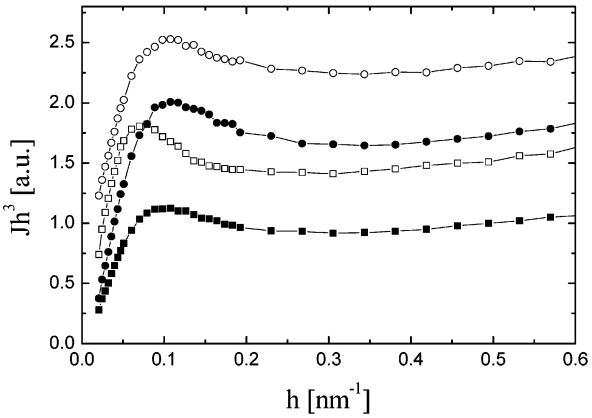

Figure 4. Porod plot of the SAXS data: ■, Lu_2O_3; □, $Lu_{1.98}Er_{0.02}O_2$; ○, $Lu_{1.98}Eu_{0.02}O_2$; ●, $Lu_{1.98}Nd_{0.02}O_2$. The locus of the first maximum of these curves defines the corresponding h_f crossover and is proportional to the size of the building unit of the mass-fractal. The curves have been vertically shifted for greater clarity.

open, polymer-like, porous microstructures produced by means of a fast cluster−cluster aggregation process.

The size of the building blocks was more precisely determined by $2\pi/h_f$, where h_f is the locus of maximum in the $J(h)h^3$ vs h plot (see Figure 4), i.e., the Porod plot for a Kratky camera.

The so-obtained particle sizes are higher than the average crystallite size values obtained by XRD (see Table 1). Such kind of differences between XRD line-broadening and SAXS size values are commonly encountered and are usually interpreted as indication for polydomain particles, i.e., single particles made up of differently oriented crystallites. Line-broadening analysis gives in fact the size of coherently diffracting domains (crystallites), whereas SAXS yields the size of areas of homogeneous electron density (particles), regardless of their crystalline structure. In the present case, however, TEM images suggest a different explanation.

In Figure 5 TEM micrographs of one of the compact area and of one of the filaments visible in the SEM

(18) Powder Diffraction File, JCPDS International Centre for Diffraction Data, Swarthmore PA, PDF no. 43-1036.

(19) *Handbook of Physics and Chemistry*, 78th ed.; Lide, D. R., Ed.; CRC Press: Boca Raton, FL, 1998; pp 4−121.

(20) Tandon, P.; Rosner, D. E. *Chem. Eng. Commun.* **1996**, *131*, 147.

(21) Martin, J. D.; Hurd, A. J. *J. Appl. Crystallogr.* **1987**, *20*, 61.

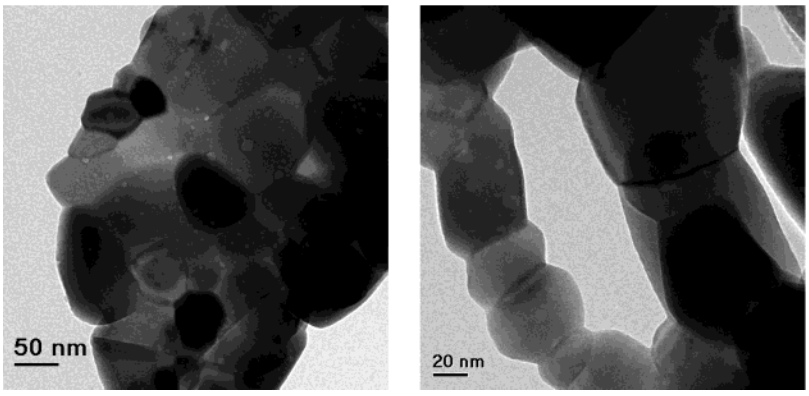

Figure 5. TEM micrographs of a $Lu_{1.98}Eu_{0.02}O_3$ sample in one of the more compact zones and in one of the filaments (see Figure 1).

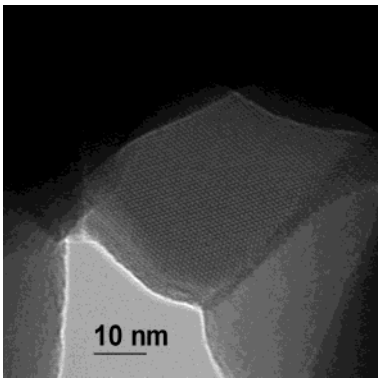

Figure 6. HRTEM micrograph of a $Lu_{1.98}Eu_{0.02}O_3$ sample showing a crystal oriented in the [111] zone-axis.

images (see Figure 1) are shown for the $Lu_{1.98}Er_{0.02}O_3$ sample. The sample is composed of interconnected particles with dimensions ranging from 30 to 100 nm. HRTEM images (see, for example, Figure 6, where one of the crystals is oriented in the [111] zone-axis) show that these particles, which are the building units of the porous structure, are single crystallites, so the difference between SAXS and XRD is not due to the polycrystalline nature of the particles. However, a careful inspection of Figure 5 shows that small voids are visible, which are probably generated by gas bubbles during the very rapid combustion process. As already observed for the previously studied yttria samples,[16,17] it is the presence of such voids that limits the size of coherence for diffraction, yielding apparent size values which are then underestimated.

Spectroscopy. Figure 7 shows the NIR luminescence of bulk and nanocrystalline Lu_2O_3:Nd^{3+} following excitation at 488 nm at room temperature. The Lu_2O_3 lattice has two distinct crystallographic sites for which the Nd^{3+} ion can substitute:[22,23] the ion can enter a site with either C_2 or C_{3i} point group symmetry. The latter site has a center of inversion, which implies selection rules forbidding all electric dipole transitions. Therefore, the 4f spectra presented in Figure 7 mainly contain electric dipole transitions from the Nd^{3+} ions sitting on the C_2 sites and magnetic dipole transitions from both sites. The spectra are composed of four distinct emission

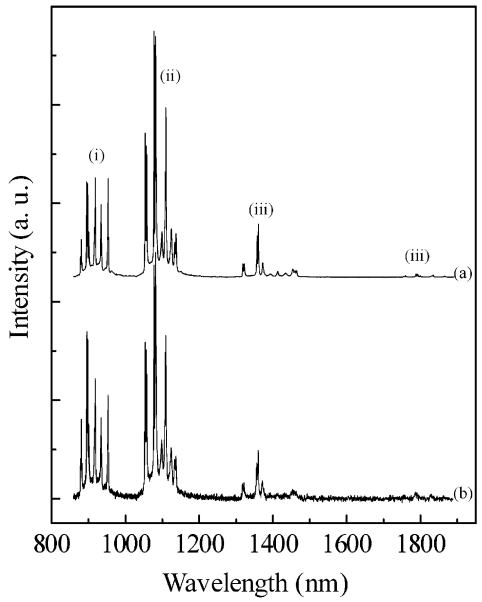

Figure 7. NIR luminescence spectra of (a) bulk and (b) nanocrystalline Lu_2O_3:Nd^{3+}, showing (i) $^4F_{3/2} \rightarrow {}^4I_{9/2}$, (ii) $^4F_{3/2} \rightarrow {}^4I_{11/2}$, (iii) $^4F_{3/2} \rightarrow {}^4I_{13/2}$, and $^4F_{3/2} \rightarrow {}^4I_{15/2}$ ($\lambda_{exc} = 488$ nm).

bands centered at approximately 920, 1100, 1400, and 1800 nm and assigned to transitions from the $^4F_{3/2}$ excited state to the lower ^4I_J states. The spectra are dominated by the bands between 860 and 980 nm, which correspond to the $^4F_{3/2} \rightarrow {}^4I_{9/2}$ transition, and between 1000 and 1200, corresponding to the $^4F_{3/2} \rightarrow {}^4I_{11/2}$ transition. Furthermore, less intense bands between 1300−1500 and 1700−1900 nm were also observed and attributed to the $^4F_{3/2} \rightarrow {}^4I_{13/2}$ and $^4F_{3/2} \rightarrow {}^4I_{15/2}$ transitions, respectively.

By comparing the NIR emission spectra of the bulk and nanocrystalline material, we observe no noticeable shift in the transition energies between the two samples, indicating that the crystal fields surrounding the ions in the two different materials are reasonably similar. However, we observed that the overall luminescence is lower in the nanocrystalline material, relative to the bulk. This behavior could be ascribed to the adsorption of atmospheric CO_2 and H_2O on the surface of the nanocrystal. As previously shown, the MIR spectrum of the undoped Lu_2O_3 nanocrystals[7] shows bands at approximately 1500 and 3300 cm^{-1}, indicating the presence of adsorbed CO_3^{2-} and OH^- species, respectively, which enter the first coordination sphere of the

(22) Wyckoff, R. W. G. *Crystal Structures*, 2nd ed.; Interscience: New York, 1964; Vol. 2.
(23) Saiki, A.; Ishizawa, N.; Mizutani, N.; Kato, M. *J. Ceram. Soc. Jpn.* **1985**, *93*, 649.

lanthanide ions that are located on the surface of the nanoparticles. Thus, the decrease of the luminescence intensity in the nanocrystalline material could be explained by the presence of carbonate and hydroxyl ions on the surface of the nanocrystals, which, due to their high vibrational energies (~1500 and ~3300 cm^{-1}), increase the probability of multiphonon relaxation. In comparison, the maximum phonon energy of lutetia (620 cm^{-1}) is available in the bulk material. This consequently minimizes nonradiative losses, thus yielding a higher luminescence.

The decay times of the $^4F_{3/2}$ level for the bulk and nanocrystalline $Lu_2O_3:Nd^{3+}$ samples were obtained by measuring the luminescence decay curves of the $^4F_{3/2} \rightarrow {}^4I_{9/2}$ transition following excitation at 488 nm. In the case of nanocrystalline $Lu_2O_3:Nd^{3+}$, the decay time of the $^4F_{3/2}$ excited is shorter (0.25 ± 0.01 ms) than that of the corresponding bulk material (0.40 ± 0.01 ms). This behavior has been observed for other trivalent lanthanide ion doped sesquioxides, for which the nanocrystalline material is usually found to have shorter decay times than the similarly doped bulk sample.[8] The total rate of depopulation of an excited state (W) is equal to the sum of the radiative decay rate (W_R), the nonradiative decay (W_{NR}), and the rate of energy transfer (W_{NR}) to another ion or to a luminescence killer such as surface defects. Clearly, the presence of the adsorbed species on the surface of the particle and the resultant large vibrational energies cause an increase in the nonradiative component, thus increasing the total rate of depopulation and in turn decreasing the observed decay time.

The NIR luminescence spectrum shows a slight broadening of the emission bands in the nanocrystalline material. Again, this is attributed to the adsorbed species on the surface of the nanocrystalline particle. Due to the small size of the particle, a larger fraction of Nd^{3+} ions are found closer to the particle surface. Thus, the crystal field surrounding these ions will be slightly different than the crystal field surrounding the ions buried in the center of the particle, and the resulting emission spectrum is a superposition of the two different Nd^{3+}environments.

Furthermore, we observed differences in the relative intensity of the $^4F_{3/2} \rightarrow {}^4I_{9/2}$ and $^4F_{3/2} \rightarrow {}^4I_{11/2}$ transitions between bulk and nanocrystalline $Lu_2O_3:Nd^{3+}$. In fact, the ratios of the integrated emission intensity of the $^4F_{3/2} \rightarrow {}^4I_{9/2}$ and $^4F_{3/2} \rightarrow {}^4I_{11/2}$ transitions are 0.825 and 0.683 for the nanocrystalline and the bulk sample, respectively. In a previous study, we showed that the NIR spectrum of nanocrystalline $Lu_2O_3:Er^{3+}$ differed significantly from its bulk counterpart. In the nanocrystalline material, the relative intensity of the $^4I_{11/2} \rightarrow {}^4I_{15/2}$ and $^4I_{13/2} \rightarrow {}^4I_{15/2}$ transitions was about 1:1, while in the bulk, the ratio was approximately 3:1. This was attributed to the presence of the adsorbed species on the surface of the nanocrystal particle, which increased the rate of multiphonon relaxation.[7] In nanocrystalline $Lu_2O_3:Nd^{3+}$, this is not the case, as we must consider that all the NIR luminescence is coming from the same initial excited state to different lower lying states. Thus, the presence of the CO_3^{2-} and OH^- groups on the surface of the nanocrystal is of little consequence in explaining the difference in the relative intensities of the $^4F_{3/2} \rightarrow {}^4I_{9/2}$ and $^4F_{3/2} \rightarrow {}^4I_{11/2}$ transitions. A very similar behavior was also observed by some of us in $Y_2O_3:Nd^{3+}$ nanocrystals, where the relative intensity of the $^4F_{3/2} \rightarrow {}^4I_{9/2}$ and $^4F_{3/2} \rightarrow {}^4I_{11/2}$ transitions was significantly higher for the nanocrystalline 10% doped $Y_2O_3:Nd^{3+}$ sample compared to the identically doped bulk material.[3]

The branching ratio $\beta_{J,J'}$ for a $J \rightarrow J'$ luminescence transition is defined as

$$\beta_{JJ'} = \frac{A(J,J')}{\sum_{J'} A(J,J')} \tag{2}$$

where $A(J,J')$ is the spontaneous emission probabilities associated with the $J \rightarrow J'$ transition and the sum is extended to all the lower lying J' levels. In the case of the Nd^{3+} ion, the intensity of the $^4F_{3/2} \rightarrow {}^4I_{J'}$ ($J' = 9/2$, 11/2, 13/2, and 15/2) transitions depend only on the Ω_4 and Ω_6 Judd−Ofelt intensity parameters given that the doubly reduced matrix element of rank 2 for transitions between these states is equal to zero.[24] Therefore, the luminescence branching ratios $\beta_{^4F_{3/2},J'}$ depend only on one parameter, $X = \Omega_4/\Omega_6$, as follows[25]

$$\beta_{JJ'}(X) = \frac{(a_J X + b_J)/\bar{\lambda}_J^{\,3}}{\sum_{J'}(a_{J'} X + b_{J'})/\bar{\lambda}_{J'}^{\,3}} \tag{3}$$

where the a_J and b_J constants are defined as the squared matrix elements of the irreducible tensor operators of rank 4 and 6

$$a_J = |\langle {}^4F_{3/2}||U^{(4)}||{}^4I_J\rangle|^2 \tag{4}$$

$$b_J = |\langle {}^4F_{3/2}||U^{(6)}||{}^4I_J\rangle|^2 \tag{5}$$

The X parameter is called the spectroscopic-quality parameter, which has been employed to study the differences in the relative $^4F_{3/2} \rightarrow {}^4I_{9/2}$:$^4F_{3/2} \rightarrow {}^4I_{11/2}$ intensities in several Nd^{3+}-doped laser crystals.[25] Each crystal has its own X parameter, which determines a set of four $\beta_{JJ'}$ coefficients. From the ratio of the integrated emission intensities of the $^4F_{3/2} \rightarrow {}^4I_{9/2}$:$^4F_{3/2} \rightarrow {}^4I_{11/2}$ emission transitions, we have obtained the X values for the bulk (0.68 ± 0.03) and nanocrystalline (0.82 ± 0.03) $Lu_2O_3:Nd^{3+}$ materials under investigation. These X values are in the range usually obtained for other oxide hosts (0.3−1.5).[25] The variation of the Ω_4/Ω_6 ratio on passing from the nanocrystalline to the bulk sample indicates that the Nd^{3+} average coordination could be different for the two materials. This could be due to the fact that in the case of the nanocrystalline material a higher fraction of the dopant ions are on the surface of the particles with respect to the bulk one, and therefore, the average crystal field experienced by the ions in the nanoparticles is different with respect to that for the bulk sample. Moreover, as discussed above, at the surface of the nanoparticles, contaminants such as

(24) Peakok, R. D. *Struct. Bonding* **1973**, *22*, 83.
(25) Kaminskii, A. A. *Laser Crystals*, 2nd ed.; Springer-Verlag: Berlin, 1990.

CO_2 and water could contribute to vary the crystal field experienced by the Nd^{3+} ion. We also note that Jorgensen and Reisfeld pointed out that the Ω_6 parameter is related to the rigidity of the host.[26] Therefore, it could be possible that the variation of the *X* parameter is correlated with a difference of the average rigidity in the nanocrystalline and bulk Lu_2O_3 host.[27]

Conclusions

Propellant synthesis is able to produce, in a very simple and economical way, porous lutetia with mass-fractal properties and nanosized building units. By simply introducing the appropriate nitrate in the starting solution, it is possible to make lanthanide-doped material with the same microstructure. Within the sensitivity of the techniques used, the lanthanide ions are homogeneously distributed within the lattice of the lutetia, giving rise to peculiar optical properties, which have been the subject of recent publications. The particular microstructure of lanthanide-doped lutetia, obtained by propellant synthesis, results in interesting properties, which make them suitable for a number of applications in the field of optical materials.

Acknowledgment. The authors are grateful to Mr. T. Finotto for the X-ray diffraction experimental work. We also thank Dr. L. Storaro for the BET measurement. This research was supported by the Italian University Ministry (Murst-National Project) and the Natural Science and Engineering Council of Canada.

CM0351240

(26) Jorgensen, K.; Reisfeld, R. *J. Less-Common Met.* **1983**, *93*, 107.
(27) Devi, A. R.; Jayasankar, C. K. *J. Non-Cryst. Solids* **1996**, *197*, 111.